ELSEVIER

Polymer 40 (1999) 5761–5771

polymer

Shearing of particles during crack growth in polymer blends

K.G.W. Pijnenburg[a], A.C. Steenbrink[b], E. Van der Giessen[a,*]

[a]*Delft University of Technology, Koiter Institute, Mekelweg 2, 2628 CD Delft, The Netherlands*
[b]*TNO Road-Vehicle Research Institute, Delft, The Netherlands*

Received 16 September 1998; accepted 14 October 1998

Abstract

Microstructural investigations below the fracture surface have revealed that the rubber particles in a number of polymer-rubber blends were deformed into remarkable S-like shapes. These shapes seem to have been largely ignored in previous microstructural studies of blends, but in fact cannot be explained from the known deformation states around a crack. We hypothesize in this paper that these shape changes develop as a consequence of macroscopic shearing of the blend as the crack front sweeps through the material. Large strain, finite element models for simple shearing of a blend are reported which demonstrate the evolution of round particles into S-shape ones for a range of material parameters, and thus support our hypothesis. The 'microscopic' localized deformation processes are identified, and the implications for the toughening mechanism in these blends is discussed.

Keywords: Cavitation; Hydrostatic tension; Plastic deformation

1. Introduction

The role of rubber particles in the toughening of amorphous or of semi-crystalline polymers is now understood quite well in a qualitative manner (e.g., [1,2]). If cavitation of the rubber particles is achieved in regions of high tensile stresses, the polymer can deform plastically by shear yielding before craze initiation can take place. Ideally, this plastic flow process is activated in the entire matrix material between the particles thus resulting in massive energy dissipation and hence increase of the fracture toughness. During this process, the cavitated particles will change substantially in shape and in volume.

As a result of the importance in the toughening process, the plastic flow around particles was studied theoretically since the 70's [3–5]. More recent studies have incorporated advanced material models for plasticity in an amorphous matrix, including the pressure dependence of yielding, intrinsic softening and orientational re-hardening at large strains [6–8]. Most of these investigations have assumed that after cavitation, the particle stiffness is so low that it is mechanically equivalent to a void, but very recently a coupled study of rubber particle cavitation and matrix plasticity was carried out [9]. All of these cited works have concentrated on the processes under macroscopic tension. This means either purely uniaxial tension or with a superimposed hydrostatic tension as is characteristic for the state of stress ahead of a crack tip. So called cavitation diagrams were constructed [9] by considering the full range of stress triaxialities.

The cited studies have all assumed that the particles are packed periodically. In real blends, this is obviously not the case, so that a precise comparison between the predicted shapes of the cavitated particles and the experimentally observed ones is difficult. Fig. 1(a) shows the distortion of some particles in polybutadiene (PB) modified styrene-acrylonitril (SAN) taken at a distance of 100 μm from the fracture surface. The smaller particles shown which have cavitated have evolved into more or less ellipsoidal shapes. Similar shapes were observed in high-impact polystyrene (HIPS) where distributed crazing is an important matrix deformation mechanism (e.g., [10]), in polycarbonate (PC) blends which deform by shear yielding only (e.g., [11,12]) and in nylon blends (e.g., [13,14]). The shapes are consistent with the predicted void shapes in [4–8] at these rather small strain levels under tension with a mild stress triaxiality. The large void visible in Fig. 1(a) has notable undulations at the interface with the matrix. This may be due to large deformations around it, as predicted in [6–8], but it cannot be ruled out that this is just caused by the clustering of a number of regular-sized particles.

In contrast with these particle shapes, Fig. 1(b) shows particles at a few particle diameters away from the fracture surface (the observation that the particles right below the

* Corresponding author. Tel.: +31-15-278-65 00; fax: +31-15-278-21-50.

E-mail address: e.vandergiessen@wbmt.tudelft.nl (E.V. Giessen)

0032-3861/99/$ - see front matter
PII: S0032-3861(98)00780-0

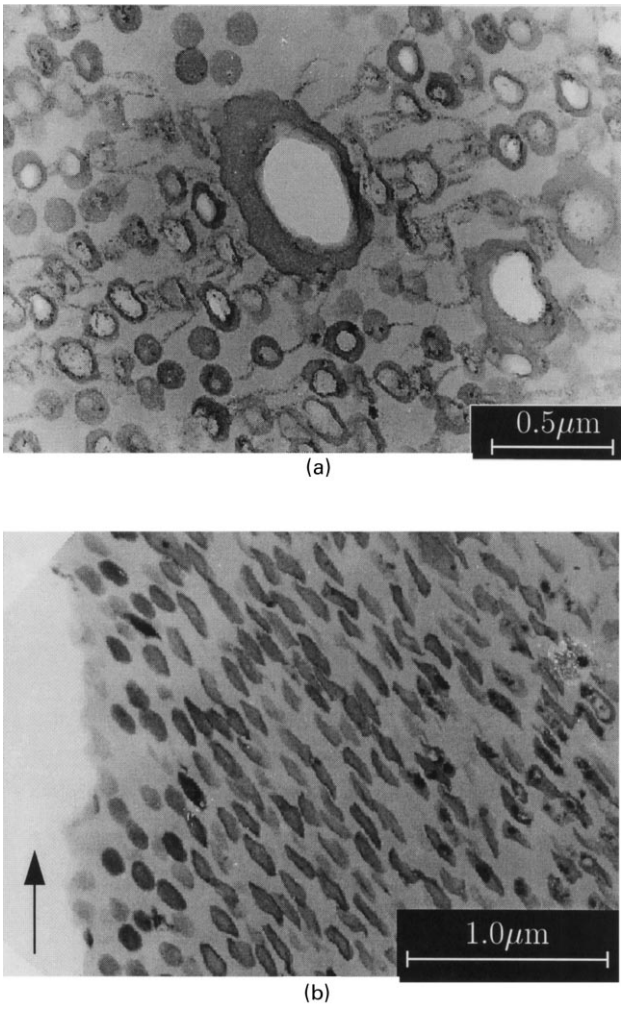

Fig. 1. TEM micrograph of a SAN-PB blend after fracture showing cavitation (white regions) in a number of smaller rubber particles. The rubber is stained in OsO_4 and appears dark grey. The SAN matrix is the lighter gray. (a) at approximately 100 μm from the fracture surface (from [7]); (b) just below the fracture surface (the arrow indicates the crack growth direction).

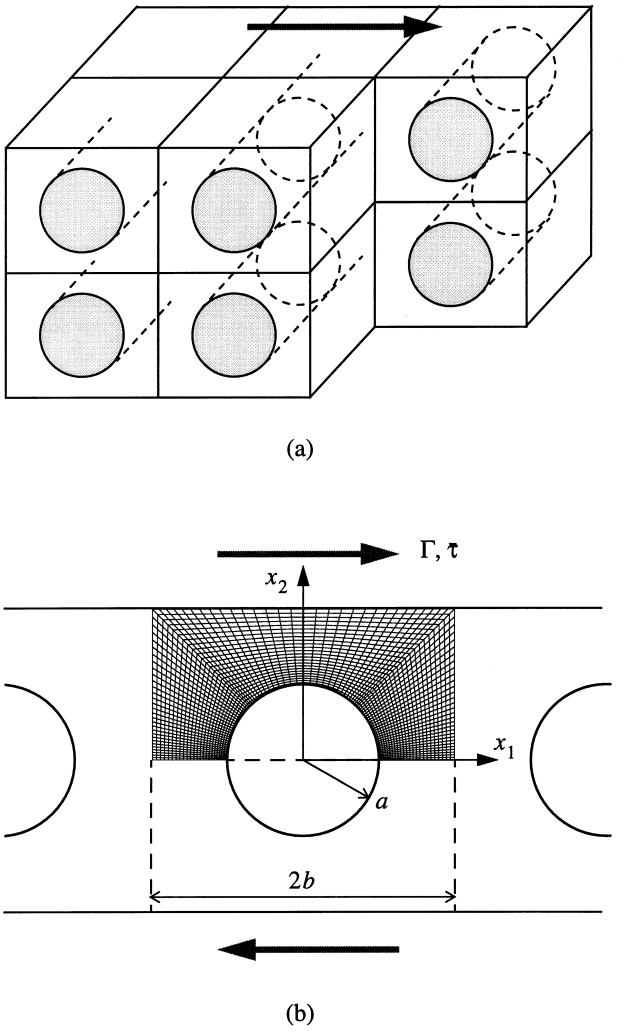

Fig. 2. (a) Model material with cylindrical particles and (b) planar unit cell model for macroscopic simple shear deformation. Only half of the unit cell needs to be analyzed due to point-symmetry. For this region, the finite element mesh is shown.

fracture surface seem hardly distorted was attributed in [15] to relaxation enabled by melting of the fracture surface). First of all, there is no visible evidence of particle cavitation, so that no significant volumetric growth can have taken place. Secondly, the elongated axis of the particles is inclined at roughly 40° to the fracture surface and not parallel to the remote tensile direction. Finally, the particles have developed into characteristic S-like shapes which are completely different from those found in Fig. 1(a). Similar shapes were found near the fracture surface in nylon-rubber blends [16,17] and to somewhat lesser extent in PC blends [18]. Highly deformed cavitated particles that are also not aligned with the tensile direction, i.e., that are not perpendicular to the fracture surface, were observed in [14] too, but they do not tend to have the typical S shape.

The origin of the particle shapes observed in Fig. 1(b) is not at all straightforward. Clearly, they involve very large strains, so that any small strain analysis would be unable to predict these shapes. But also all large strain studies known to the authors have never predicted shapes like these, not even for the full range of stress triaxialities considered in [9]. It is highly unlikely that the absence of predictions is due to the assumed periodicity of the particle arrangement in these theoretical studies. The particles seen in Fig. 1(b) are obviously not periodically ordered, but they are not clustered in any way that could explain the discrepancy. Another more implicit assumption in the theoretical studies was that the macroscopic deformation pattern possesses orthorhombic symmetries. In a planar view, this means that there are two orthogonal planes of symmetry, or two two-fold symmetries. This is a very common and well-established assumption in the micromechanics of damage solids for predominantly tensile loading. However, the particle shapes in Fig. 1(b) do not have this symmetry, but at best only one-fold symmetry or inversion symmetry.

These considerations lead us to the hypothesis that the

S-shape of the particles has evolved during a macroscopic simple shear process. This is a distinctly different deformation mode than pure shear, which can be decomposed into two orthogonal tensile stretch processes and therefore possesses orthorhombic symmetry. Simple shear involves stretching and material rotation of equal magnitude, and respects only inversion symmetry. This hypothesis is tested by a specially designed unit cell analysis, which is outlined in Sec. 2. The results obtained from numerical computations with this model (Sec. 3) are then discussed (Sec. 4) in the light of the characteristics of simple shearing and compared with what one finds under pure shear deformation. From this, we conclude with speculating on the deformation modes around a propagating crack in a polymer blend (Sec. 5).

2. Model for simple shear of blend

In order to avoid the computational burden of three-dimensional computations, we consider a model material that is essentially two dimensional. In the undeformed state of the material, the rubber particles have a circular cylindrical shape, have identical size and are arranged in a square array as illustrated in Fig. 2(a). If, in the undeformed state, the particle radius is a and $2b$ is the spacing between particles, the area fraction of particles in a cross-section is $f = (\pi/4)(a/b)^2$. To test our hypothesis, we imagine that the material is subjected to macroscopic simple shear in the x-direction parallel to the particle lattice. If the material would be homogeneous, the deformation would be uniform. Then, the rate of change dv_i $(i = 1, 2)$ of all line element dx_i would be given by the same velocity gradient L_{ij} according to $dv_i = L_{ij}dx_j$ (summation over repeated indices implied). For simple shear, the components L_{ij} with respect to the (x_1, x_2) axes in Fig. 2(a) are of the form

$$(L_{ij}) = \begin{pmatrix} 0 & \dot{\Gamma} \\ 0 & 0 \end{pmatrix}, \tag{1}$$

with $\dot{\Gamma}$ the shear rate. The corresponding components of accumulated strain, E_{ij}, and of stress, Σ_{ij}, read

$$\left(E_{ij}\right) = \begin{pmatrix} 0 & \frac{1}{2}\Gamma \\ \frac{1}{2}\Gamma & 0 \end{pmatrix}, \qquad \left(\Sigma_{ij}\right) = \begin{pmatrix} 0 & \bar{\tau} \\ \bar{\tau} & 0 \end{pmatrix} \tag{2}$$

with Γ the accumulated shear strain and $\bar{\tau}$ the shear stress. In the composite material considered here, the fields are not uniform, and those in Eq. (2) represent the overall or macroscopic strain and stress.

As a result of of periodicity, we only need to consider a $2b \times 2b$ unit cell containing a single particle (see Fig. 2(b)). When we further make use of inversion symmetry about the center of the particle, we only need to consider half of this cell. As the deformations are expected to be confined mainly to the ligament between particles (as indeed the results will confirm), one would expect that the shear deformations near the top or bottom of the unit cell are also almost uniform. Therefore, we may simply apply the simple shear loading through prescribed displacements on the top (and bottom) of the unit cell. With the origin of the (x_1, x_2) coordinate system at the particle center, the boundary conditions in terms of velocities v_i are

$$v_1 = b\dot{\Gamma}, \; v_2 = 0 \qquad \text{along } x_2 = b, \; -b \le x_1 \le b$$

with Γ the overall or macroscopic shear and the superposed dot denoting the time derivative. The macroscopic response will be monitored by the average $\bar{\tau}$ of the shear stress σ_{12} either along the top edge,

$$\bar{\tau} = \frac{1}{2b}\int_{-b}^{b} \sigma_{12}(x_1, b)\mathrm{d}x_1,$$

or along the bottom edge $x_2 = -b$ (by virtue of equilibrium, the two are identical). The remaining 'boundary conditions' are periodicity along the sides of the cell, $v_i(b, x_2) = v_i(-b, x_2)(|x_2| \le b)$, and inversion symmetry, $v_i(x_1, 0) = -v_i(-x_i, 0)$, along $a \le |x_1| \le b$.

Homogeneous shearing is a volume-preserving deformation mode, i.e., $E_{kk} = 0$ according to Eq. (2). Hence, one expects that the particle will be distorted mainly in shape even if it would have a very low bulk modulus. Since the shear modulus of rubbers are usually one to two orders of magnitude smaller than the yield stress of the polymer matrix, also the effect of shear deformations of the rubber particle can be neglected. The rubber particle therefore appears to be mechanically equivalent to a void under shear deformations. Therefore, we actually replace the particle with a traction-free void. The computations to be presented later have confirmed that the volume change of the void is negligible compared to the overall shear strain Γ.

The material model used here was developed explicitly for amorphous glassy polymers. It accounts for rate-dependent shear yielding, the intrinsic softening that immediately follows yield in amorphous polymers and the subsequent strain hardening due to the stretching of the entanglement network. The model closely follows the original ideas put forward in one dimension by Haward and Thackray [19] in which the strain hardening is represented by a Langevin spring in parallel to a yielding element. The three-dimensional theory that we use is based on work by Boyce et al.

Table 1
The three sets of material parameters used in this study. The names are for identification only; the parameter values are not intended to represent specific materials

	E/s_0	ν	s_{ss}/s_0	As_0/T	h/s_0	α	N	C^R/s_0
SAN	12.6	0.38	0.79	52.2	12.6	0.25	12.0	0.033
PC	9.4	0.3	0.79	79.2	5.15	0.08	6.3	0.059
Nylon	29.7	0.41	1.0	77.0	0.	0.08	16.0	0.021

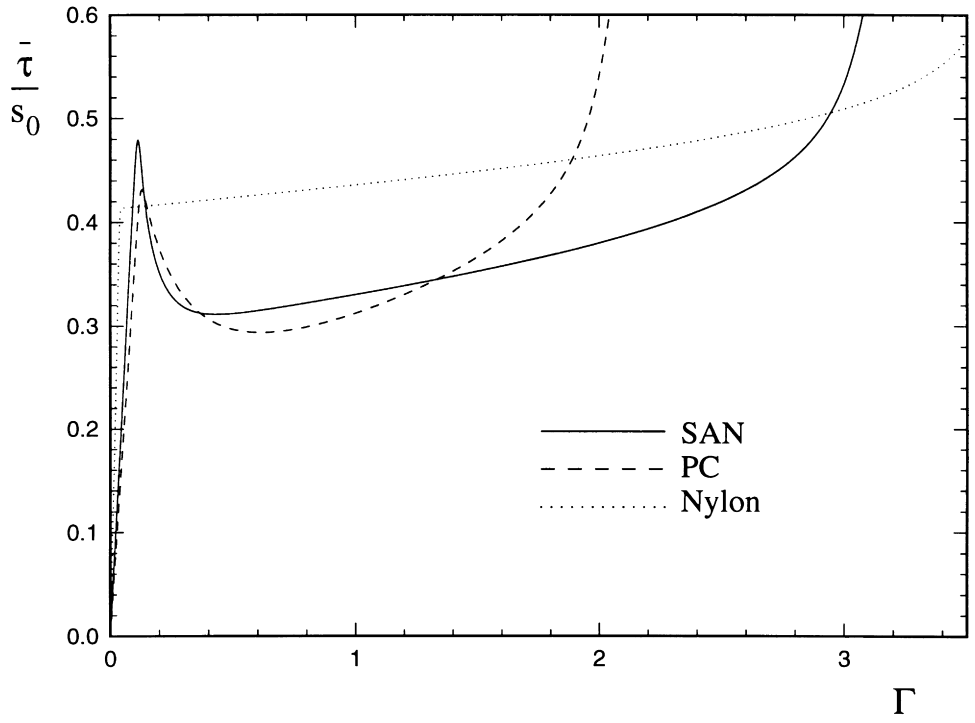

Fig. 3. Shear stress (τ) vs shear strain (Γ) response according to each of the three sets of parameters in Table 1 to homogeneous simple shear, i.e., in the absence of particles or voids. The shear stress is normalized by the athermal shear strength s_0 of the material.

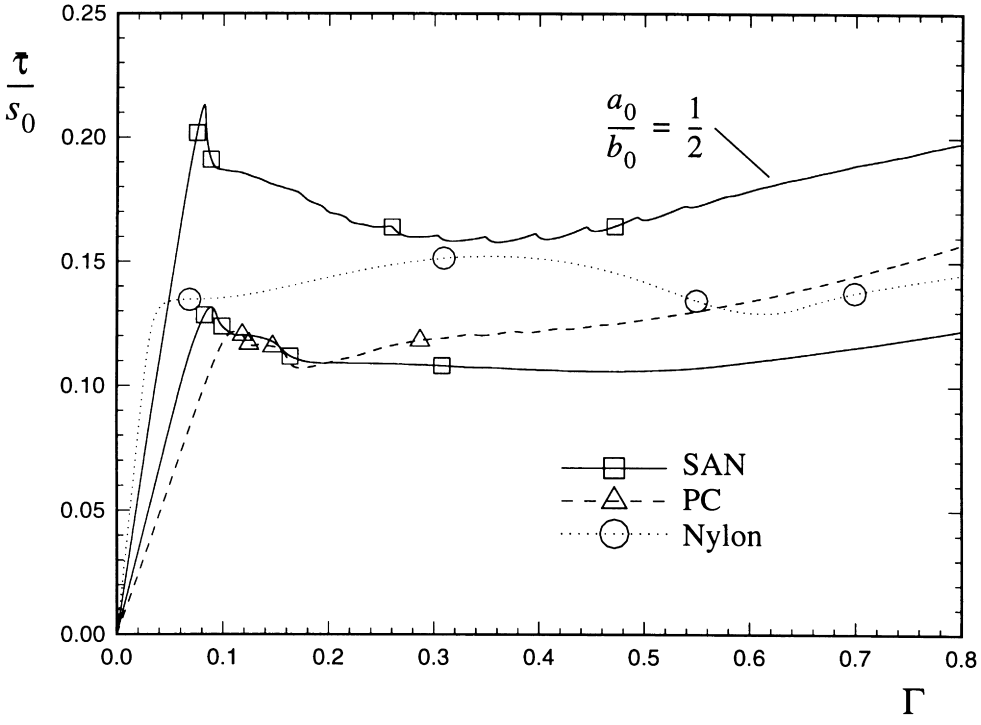

Fig. 4. Average shear stress ($\bar{\tau}$) vs applied shear strain (Γ) for the three blends with particles/voids of size $a/b = 2/3$. For SAN, results are also shown for $a/b = 1/2$. The shear rates are the same as in Fig. 3. Symbols refer to the plots in Figs. 5–8.

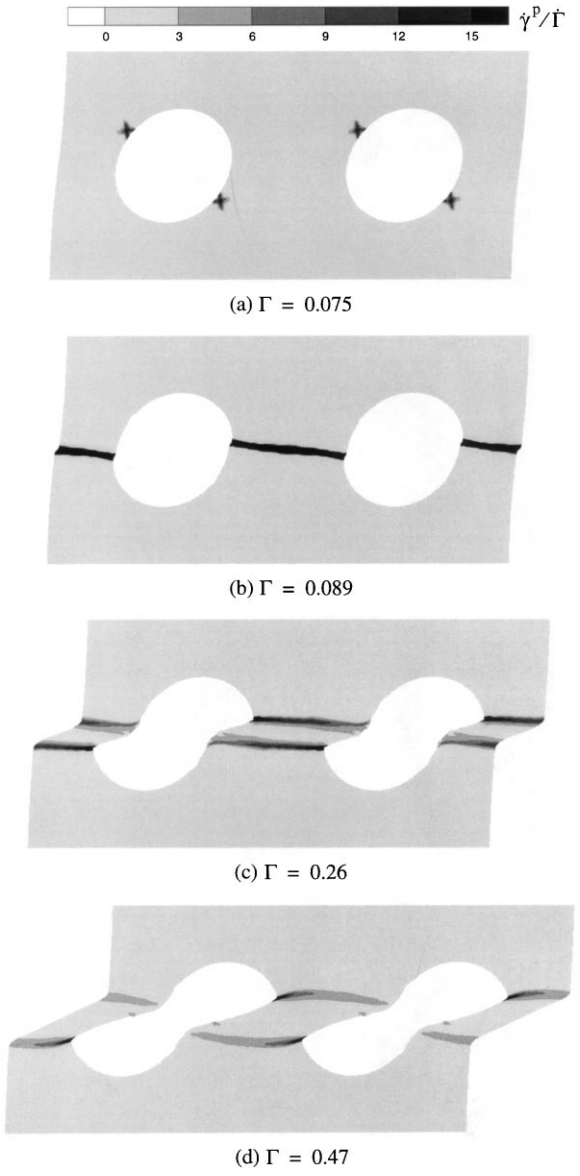

Fig. 5. Distribution of local plastic shear rate $\dot{\gamma}^p$ at various stage of macroscopic strain Γ in the SAN blend with $a/b = 1/2$. The plastic shear rates are normalized with the macroscopic shear rate $\dot{\Gamma}$.

[20], but employs the slightly modified version developed in [21].

Rate-dependent yielding is taken to be described by the expression

$$\dot{\gamma}^p = \dot{\gamma}_0 \exp\left[-\frac{As_0}{T}\left(1-\left(\frac{\tau}{s_0}\right)^{5/6}\right)\right], \tag{3}$$

derived by Argon [22] for the plastic shear-rate $\dot{\gamma}^p$ as a function of the driving shear stress τ. Here, $\dot{\gamma}_0$ is pre-exponential factor, A is a material parameter that is proportional to the activation volume, T is the absolute temperature and s_0 is the athermal shear strength. Boyce et al. [20] extended this expression in a phenomenological way to include the effect of pressure and strain softening. They use $s + \alpha p$ instead of s_0, where p is the pressure and α is a pressure dependence coefficient. Furthermore, s is assumed to evolve with plastic straining from the initial value s_0 to a steady-state value s_{ss}, via

$$\dot{s} = h(1 - s/s_{ss})\dot{\gamma}^p, \tag{4}$$

to incorporate a phenomenological description of softening. The rate of softening is governed by the material parameter h.

The driving shear stress τ in the flow rule Eq. (3) is determined in the three-dimensional theory from

$$\tau = \sqrt{\frac{1}{2}\bar{\sigma}'_{ij}\bar{\sigma}'_{ij}}, \quad \bar{\sigma}_{ij} = \sigma_{ij} - b_{ij}, \quad \bar{\sigma}'_{ij} = \bar{\sigma}_{ij} - \frac{1}{3}\bar{\sigma}_{kk}\delta_{ij}$$

where σ_{ij} is the local stress tensor and b_{ij} is the back stress ($i,j = 1,2,3$ and δ_{ij} is the Kronecker delta). The back stress is an internal stress associated with the stretching of the entanglement network upon continued plastic deformation. Following the suggestion in [19], this back stress is modeled using non-Gaussian network theory. Thus, its principal components b_i have the same directions as the plastic stretch, and are direct functions of the corresponding principal plastic stretches λ_α. It was shown by Wu and Van der Giessen [21] that the predictions of the full (or random) network theory could be captured accurately in terms of a simple combination of the classical three-chain network description and the Arruda–Boyce [23] eight-chain model:

$$b_i = (1-\rho)b_i^{3-ch} + \rho b_i^{8-ch}, \tag{5}$$

with ρ being determined by the maximum plastic stretch $\bar{\lambda} = \max(\lambda_1, \lambda_2, \lambda_3)$ through $\rho = 0.85\bar{\lambda}/\sqrt{N}$. Here, N is a statistical network parameter, which gives the average number of links between entanglements (or cross-links in rubber) and thus determines the limit stretch $\lambda_{\max}$ of a molecular chain as $\lambda_{\max} = \sqrt{N}$. The principal back stress components b_i^{3-ch} and b_i^{8-ch} are given by

$$b_i^{3-ch} = \frac{1}{3}C^R\sqrt{N}\lambda_i\mathscr{L}^{-1}\left(\frac{\lambda_i}{\sqrt{N}}\right), \tag{6}$$

$$b_i^{8-ch} = \frac{1}{3}C^R\sqrt{N}\frac{\lambda_i^2}{\lambda_c}\mathscr{L}^{-1}\left(\frac{\lambda_c}{\sqrt{N}}\right); \quad \lambda_c^2 = \frac{1}{3}\sum_{j=1}^{3}\lambda_j^2, \tag{7}$$

where $\mathscr{L}^{-1}$ is the inverse of the Langevin function $\mathscr{L}(\beta) = \coth\beta - 1/\beta$. The material parameter C^R is termed the hardening modulus (in rubber elasticity, it is the shear rubbery modulus). When the value of either $\bar{\lambda}$ or λ_c approaches $\lambda_{\max}$, the hardening rate increases dramatically, thereby effectively 'locking' the material for further flow. The material model is implemented in finite element code that duly accounts for large stain effects. The finite element mesh used for this problem with a relative void size of $a/b = 0.5$ is shown in Fig. 2. Further details on the material model and the finite element formulation may be found in [6,21]. We only note that special care is needed in computations of

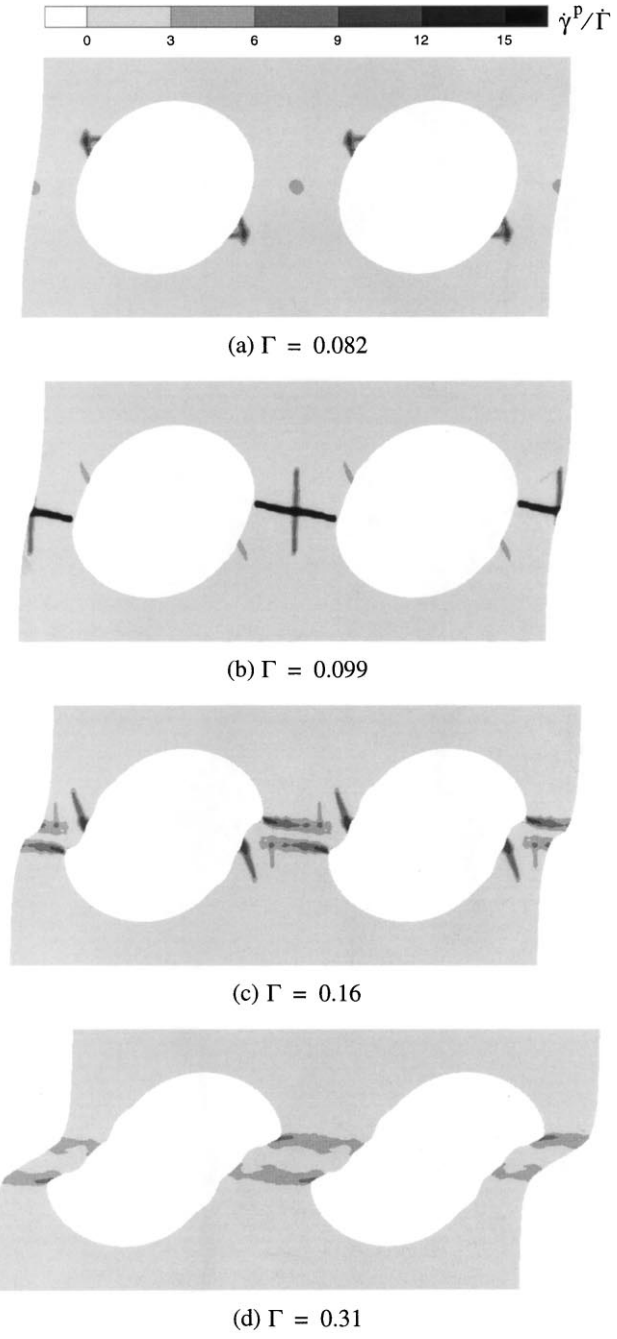

Fig. 6. Distribution of normalized local plastic shear rate $\dot{\gamma}^p$ at various stages of macroscopic strain Γ in the SAN blend with $a/b = 2/3$.

this type in order to keep them numerically stable. When this is properly done, the material model has been shown to be able under various deformation conditions to describe the initiation of shear bands and their subsequent propagation typical for amorphous glassy polymer (e.g., [6]).

3. Results

Calculations were carried our for different initial void sizes, as expressed by the ratio a/b, and for various sets of material parameters. Results will be presented for values of a/b of 1/2 and 2/3, corresponding to initial volume fractions f of approximately 20% and 35%, respectively. The three sets of material parameters used in this study are listed in Table 1. Although they do not represent actual material, the three sets will be referred to as SAN, PC or Nylon, since these sets give large strain responses that are characteristic of these materials. The SAN data set gives rather strong softening upon yield, the PC data yield somewhat less softening and smaller limit strain, while the Nylon data set predicts no softening at all after yield (see Fig. 3). The strain-rate dependence is governed by the value of $\dot{\gamma}_0$ relative to the applied shear rate $\dot{\Gamma}$: $\dot{\Gamma}/\dot{\gamma}_0 = 9.43 \times 10^{-11}$ for SAN, and 5.0×10^{-18} for PC and Nylon.

Fig. 4 shows the computed stress-strain curves for the three materials with voids. The decrease in macroscopic yield stress compared to the yield stress of the corresponding matrix material is obvious. Quite interestingly though, the presence of the voids has significantly changed the differences among the three materials seen in Fig. 3, and has effectively eliminated their limited deformability. This change is connected to the differences in how local plasticity evolves around the voids for the three materials. In order to study this in more detail, Figs. 5–8 show contour plots of the plastic shear rate $\dot{\gamma}^p$. These plots illustrate the development of the current plastic zone around the voids with ongoing overall straining.

It is seen from Figs. 5(a) and 6(a) that plasticity first begins in the form of two crossed short shear bands near the void surface at an angle of approximately $-45°$ to the shear direction. The shear bands are an immediate consequence of the intrinsic softening upon yield in SAN. Due to the constraint of surrounding material, this plastic flow is confined to a small region and soon dies out. Then, plasticity inside the ligaments between voids is activated. It initiates in the center and rapidly evolves into a rather thin band across the entire ligament (Figs. 5(b) and 6(b)). Very similar shear band formation is also found in the other two materials (PC: Fig. 7(a); Nylon: Fig. 8(a)).

Once the ligament has yielded, further deformation of the material can be accommodated entirely by plastic shearing inside these shear bands, especially of the materials that exhibit significant strain softening after yield (i.e., SAN and PC). In these materials, this ligament shearing therefore results in a reduction of the overall macroscopic stress level (Fig. 4). Localized shearing continues until the strains inside the band become so large that the molecular chains become extended and hardening sets in, just like in homogeneous shearing (Fig. 3).

Once hardening has developed to a sufficient level, neighboring material becomes prone to yield. Due to the simultaneous softening inside this region and the further hardening of the material inside the original shear band, the latter can no longer flow and locks up. As a result, localized shearing is now confined to two shear bands on

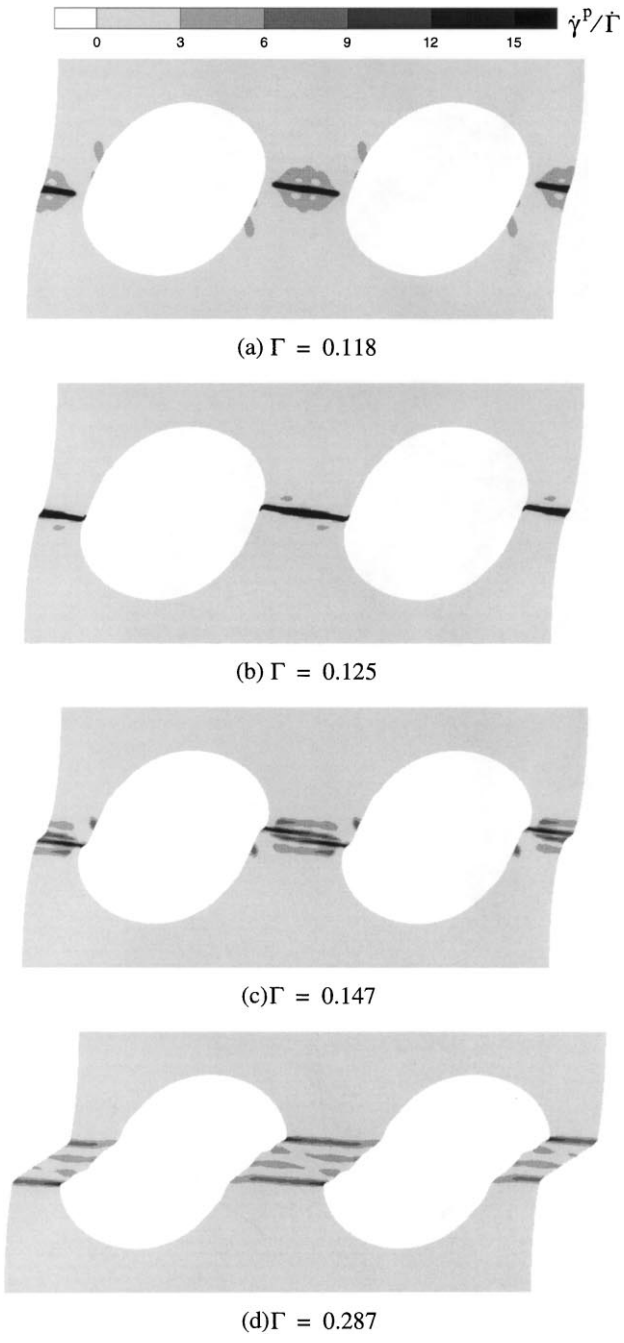

Fig. 7. Distribution of normalized local plastic shear rate $\dot{\gamma}^p$ at various stages of macroscopic strain Γ in the PC blend with $a/b = 2/3$.

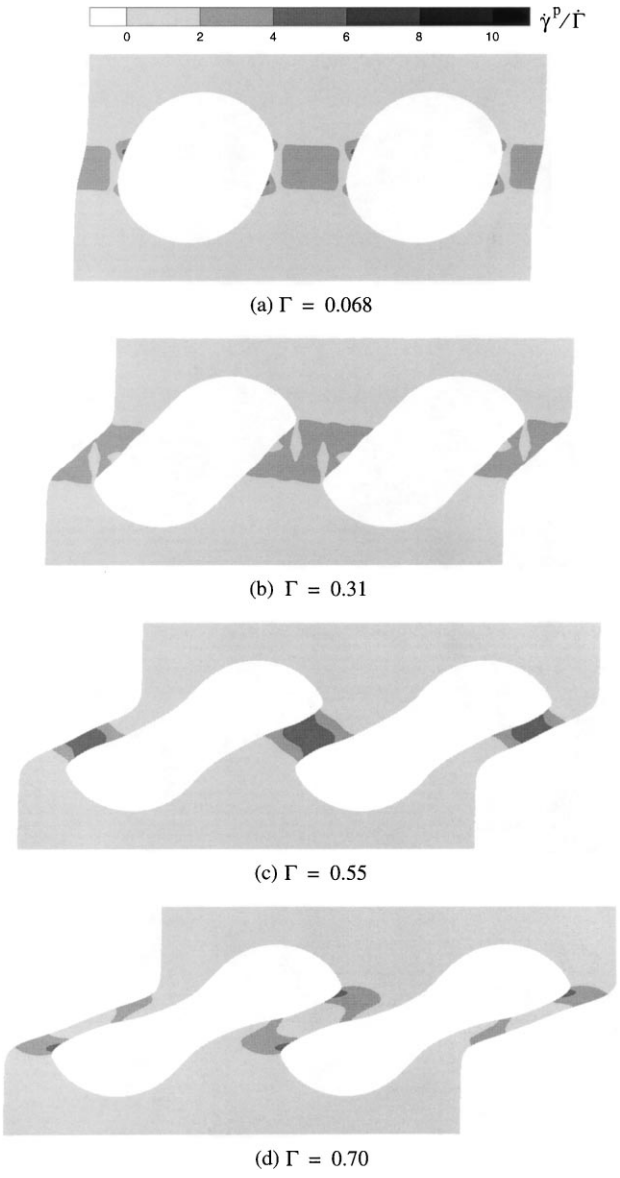

Fig. 8. Distribution of normalized local plastic shear rate $\dot{\gamma}^p$ at various stages of macroscopic strain Γ in the Nylon blend with $a/b = 2/3$.

either side of the original one. This is most clearly seen for SAN with $a/b = 1/2$ in Fig. 5(c). The process of yielding, flowing and hardening can then repeat itself and causes the shear bands to propagate perpendicular to the shearing direction, so as to leave a band of sheared material with increasing width. This trend is observed more or less neatly for all cases analyzed, although also other shear bands are initiated for the larger value of a/b (last snapshots of Figs. 5–8).

In all cases, the voids take on an elongated S-like shape at large shear strains. The longest axis starts out at an angle of 45° to the shearing direction and this orientation gradually rotates with continued shearing. It is clear from the Figs. 5–8 that the S-shape is a direct consequence of the propagative shear bands between voids. At the surface of the voids, where a shear band in the matrix terminates, a kink is visible. The sharpness of this kink depends primarily on the level of localization in shear bands, which in turn is controlled by the amount of softening experienced by the material. The larger the softening (in ascending order: Nylon, PC, SAN), the sharper the kink is.

The results presented for SAN in Figs. 5 and 6 show that the void evolution does not depend significantly on the ratio a/b or, equivalently, on the normalized inter-particle distance $(b - a)/b$. The reason is that there is no overlapping

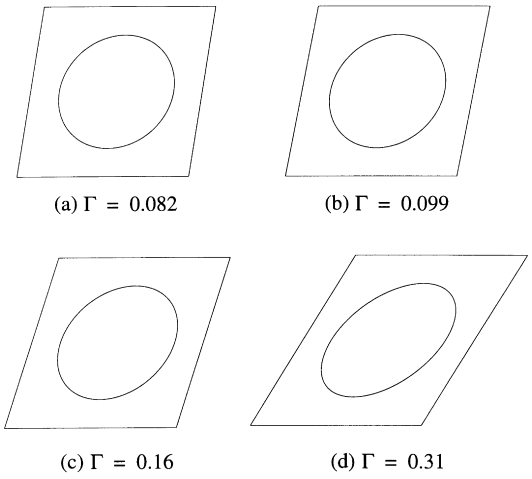

Fig. 9. Evolution of a circle on a material that deforms by uniform simple shear at various overall shear strains Γ (cf. Fig. 6).

of or interaction between shear bands that depends on the width of the ligament, $b - a$. Within reasonable bounds on a/b, materials with a different ligament size exhibit the same stages of localized deformation, although, of course, at different levels of stress and strain (Fig. 4).

In all cases, the change in volume of the voids remained smaller than about 1%, except for SAN where volume increases of up to 4% were observed, but only at the largest strains. This justifies our approximation of replacing rubber particles by voids.

4. Discussion

Local plasticity has been seen to initiate (Figs. 5(a), 6(a)) prior to macroscopic yielding (cf. Fig. 4). Macroscopic yield occurs by a shear band that connects adjacent voids. A simple estimate of the macroscopic yield stress $\bar{\tau}_y$ can be obtained by equating the average shear stress over the ligament between voids, $\bar{\tau}_{\text{lig}}$, to the intrinsic shear yield stress τ_y, of the matrix material at the macroscopic shear rate. It follows from equilibrium that $\bar{\tau} = (1 - a/b)\bar{\tau}_{\text{lig}}$, so that the macroscopic yield stress can be estimated as $\bar{\tau}_y = (1 - a/b)\tau_y$. With an intrinsic yield stress $\tau_y \approx 0.4s_o$ (Fig. 3), the macroscopic yield stress in a blend with $a/b = 1/2$ is approximately $\bar{\tau}_y = 0.2s_0$, while it is $\bar{\tau}_y \approx 0.13s_0$ when $a/b = 2/3$. These estimates agree rather well with the numerical values in Fig. 4.

It was mentioned in the previous section that the typical S-shape of the voids is a consequence of the propagating shear bands under overall simple shear. To emphasize the role of the shear bands, Fig. 9 shows the evolution of a circular region of a homogeneous material under (uniform) simple shear. This is identical to the case where the properties of the particles are identical to those of the matrix. The deformed shape is governed directly by the time integral of the velocity gradient in (1). It shares with the computed void shapes in Figs. 5–8 the characteristic feature that it elongates and rotates towards the shearing. However, it cannot but retain an elliptical shape. The S shape requires significant localized deformations.

Moreover, the overall deformation must contain a significant rotation. Simple shear is a deformation process in which the average rate of rotation is equal to the average rate of straining. In order to demonstrate the necessity of material rotation, we shall briefly consider the same model material as in Fig. 2(a) but subjected to pure shear, as illustrated in Fig. 10. The velocity gradient for pure shear reads

$$\left(L_{ij}\right) = \begin{pmatrix} 0 & \dot{\Gamma}/2 \\ \dot{\Gamma}/2 & 0 \end{pmatrix}, \tag{8}$$

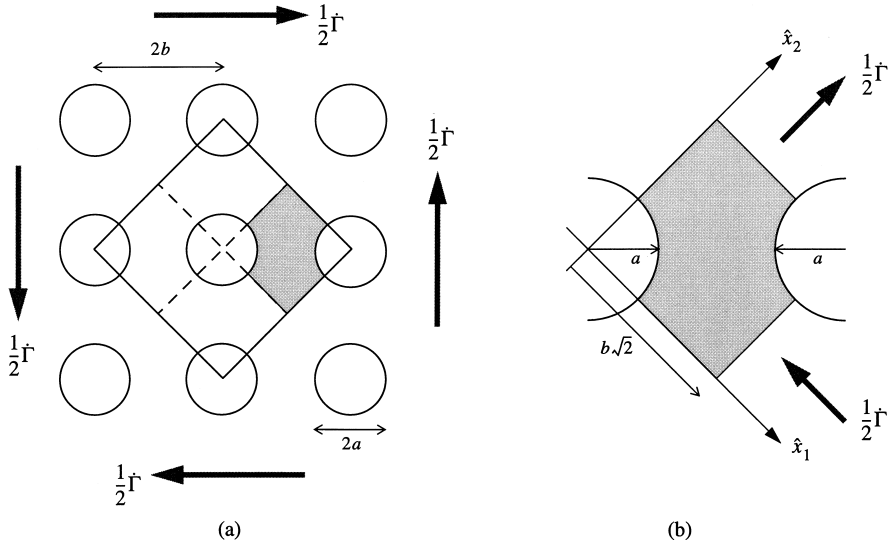

Fig. 10. (a) Model material subjected to pure shear. As a result of of two-fold symmetries only a quarter of the unit cell (hatched) needs to be analyzed. (b) equivalent quarter cell subject to equal tension-compression.

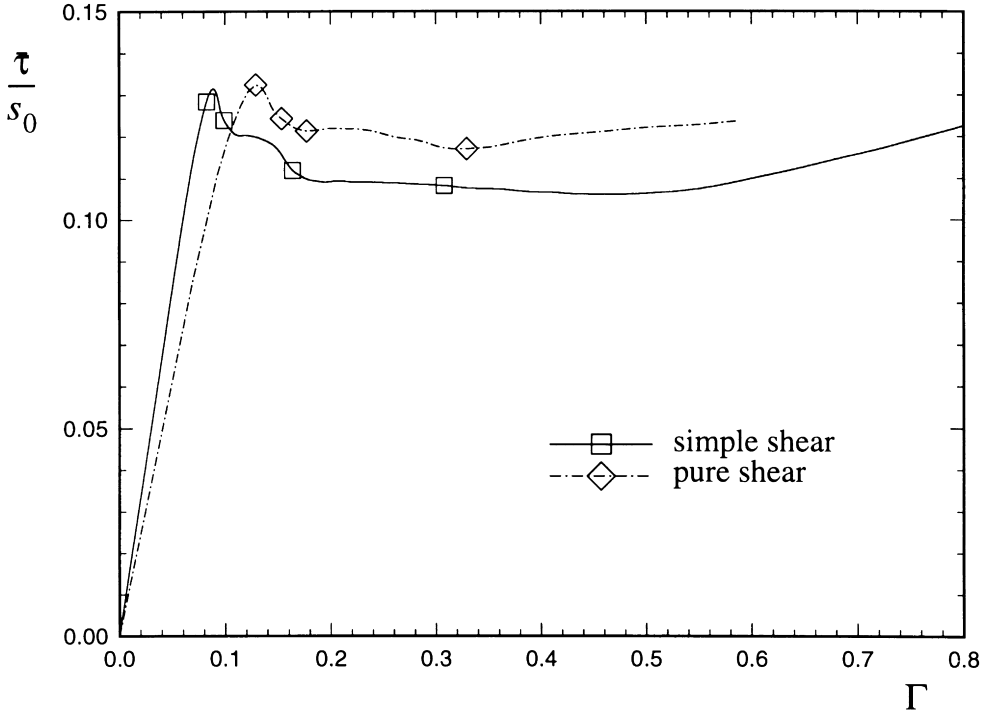

Fig. 11. Average shear stress response to pure shear vs simple shear for the SAN blend with $a/b = 2/3$. The □'s refer to Fig. 6 and the ◇'s to Fig. 12.

as opposed to the simple shear expression Eq. (1). Hence, pure shear does not contain a rate of rotation but the accumulated strain is the same as under simple shear, see Eq. 2(a). As shown in Fig. 10(a), the material under this loading configuration has additional two-fold symmetry in diagonal directions. As a consequence, it is possible to identify another unit cell, oriented at 45°. With respect to associated local axes $\hat{x}_i$ (see Fig. 10(b)), the velocity gradient transforms into

$$\left(\hat{L}_{ij}\right) = \begin{pmatrix} -\dot{\Gamma}/2 & 0 \\ 0 & \dot{\Gamma}/2 \end{pmatrix}, \tag{9}$$

so that the pure shear problem is equivalent to normal tension in the $\hat{x}_2$ direction and simultaneous compression of the cell in the $\hat{x}_1$ direction. The latter problem (Fig. 10(b)) is of the type analyzed previously in [6,8]. With reference to these cited works for the method of analysis, we show results for this problem for the SAN parameter set and with $a/b = 2/3$ in Figs. 11 and 12.

The stress-strain curves show that the macroscopic yield stress under pure shear deformations is roughly the same as that for simple shear (the fact that the elastic stiffness under pure shear is slightly different from that under simple shear is a second-order effect due to the kinematic constraint in the x_2 direction imposed by simple shear, which vanishes for small void volume fractions). However, the stress drop after yield is less distinct than under simple shear, and this is caused by a different post-localization behaviour. There are similarities in the types of shear bands formed at the respective yield points, cf. Fig. 6(a) with Fig. 12(a), although under pure shear more sets of shear bands are needed to accommodate the deformation. Continued deformation under pure shear (Fig. 12(b),(c)) leads also to the initiation and propagation of shear bands across the ligaments, but not only in the horizontal direction as in simple shear (Figs. 6(b),(c)) since also the corresponding vertical shear bands are needed for symmetry. As a consequence, the shape changes of the void/particle (Fig. 12(d)) retain two two-fold symmetries and are therefore distinctly different from the S-shapes predicted under simple shear (Fig. 6(d)). Apparently, it is the rotation implied in simple shear that breaks the symmetry and therefore allows the material to develop the S-shape voids/particles.

5. Implications and Conclusion

The results presented in Sections 3 and 4 confirm our hypothesis that the S-shaped particles seen just below the fracture surface in ABS (Fig. 1(b)) are due to macroscopically large strain simple shear of the blend. This is quite remarkable, since such deformation modes are rather seldomly observed in the fracture of materials, at least at a macroscopic scale. Fracture of ductile crystals of metals do show intense shear banding, but this happens at the scale of nanometers and is caused by discrete slip processes on well-defined crystallographic planes. Also, for the type of blends considered here, shear banding is not the only deformation mode. Usually, the cavitated particles at some distance

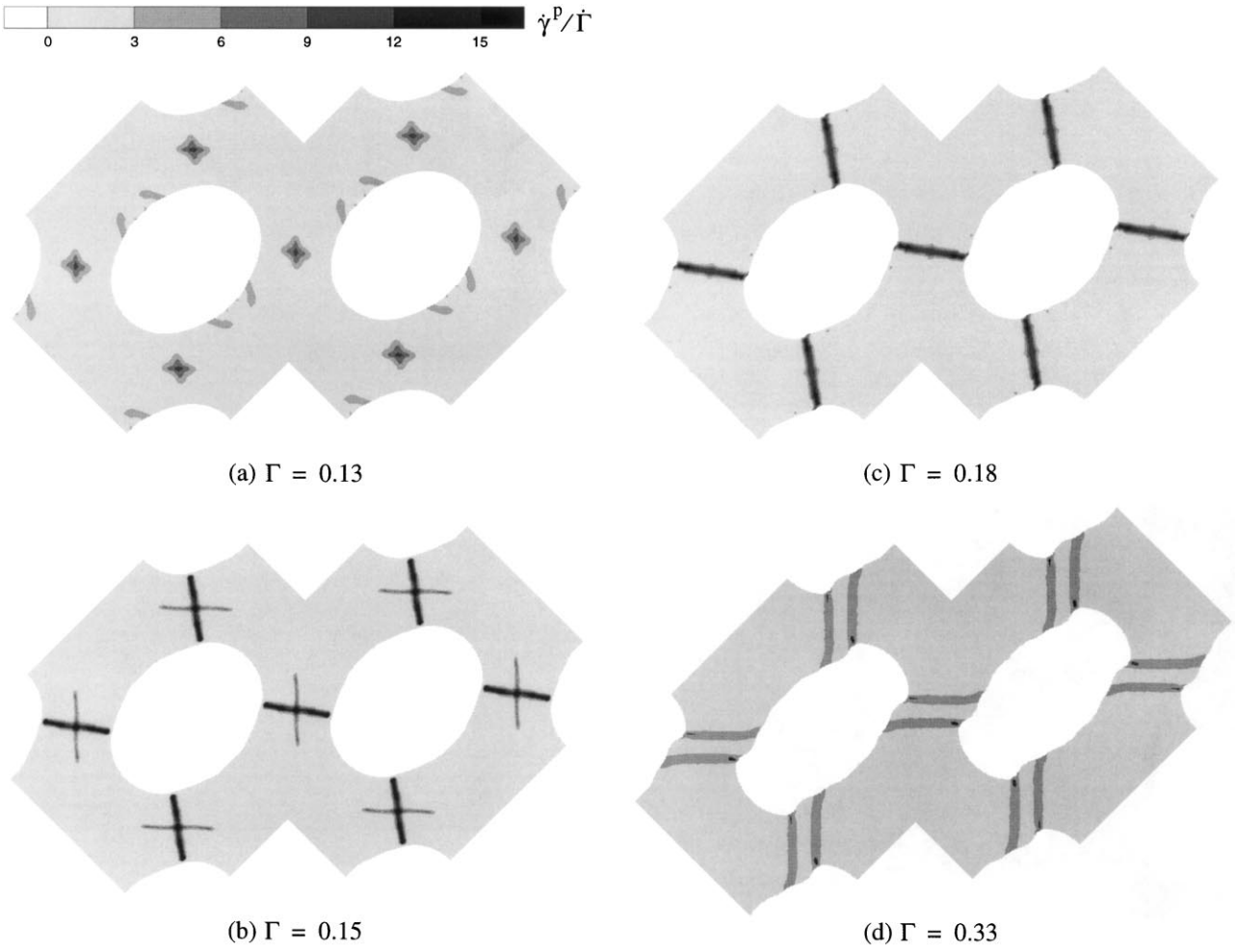

Fig. 12. Distribution of normalized local plastic shear rate $\dot{\gamma}^p$ at various stages of macroscopic strain Γ in the SAN blend with $a/b = 2/3$ under pure shear. The corresponding simple shear results are in Fig. 6.

ahead of the crack tip have a more or less elongated shape (see e.g., Fig. 1(a)), as mentioned in the Introduction. On the basis of these observations we now speculate (see Fig. 13) that ahead of the tip of a propagating crack in a blend showing deformed particles as in Fig. 1(b) there will be a region of predominant macroscopic tension (with elongated, cavitated particles) and a region of intense shearing behind the moving crack tip (with S-shaped particles). In between, there will be a complex transition region.

The existence of two such regions may have a significant influence on the toughening effect of the particles in such a blend. As is generally accepted now, the function of the particles in the first, tensile, region is to prevent crazing of the matrix and to trigger plastic yielding. However, as the deformations in the second region can become very large, a significant part of the actual energy that is dissipated during crack extension can be expended in the shear region behind the crack tip. Though counterintuitive this may be, nonlinear fracture mechanics has in fact identified a number of material systems over the last decade that owe their toughness to processes taking place in the wake of the

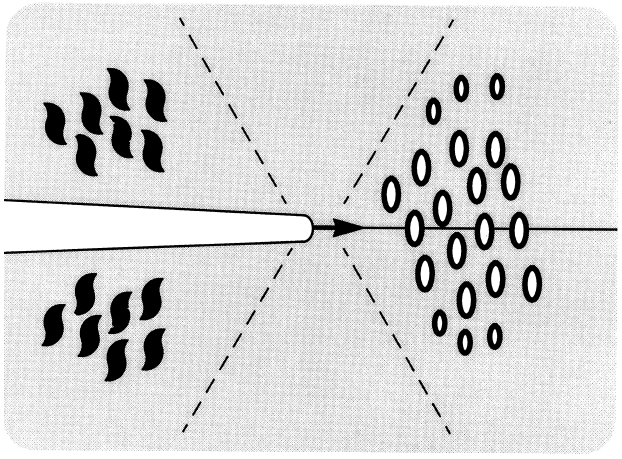

Fig. 13. Schematic of the suggested existence of distinctly different zones around a propagating crack in some polymer blends: a tensile region ahead of the tip, where particles cavitate and deform into elongated shapes and a shear region in the wake of the crack. The transition in between is unclear at this stage.

crack. A typical example is zirconia-toughened ceramics. In this material, toughening is caused by the strains caused by a phase transformation behind the crack tip; the transformation in front of the crack actually tends to embrittle the material [24].

In view of the relatively small number of reports in the open literature about S-shaped particles below the fracture surface, it is likely that an intense shear region in the wake of the crack will occur only in certain blends. The question as to when it takes place cannot be easily answered. The reason is that it is far from being trivial to see why and how the transition from tensile-dominated deformations to shearing takes place as the crack grows. This transition is not only controlled by the stress state behind the crack but by the entire stress and deformation fields around the moving crack tip. These in turn are controlled by the overall behaviour of the blend, including particle cavitation and plasticity in the cavitated material. These fields are totally unknown at the moment. Theoretical confirmation of the speculated picture in Fig. 13 thus requires analysis of the full crack growth problem in a material exhibiting this specific material behaviour. Experimental confirmation may be possible by application of a 'grid' with a spacing on the order of the particle spacing, so that the history of strain and of rotation (indicative of simple shear) can be followed.

References

[1] Bucknall CB. Toughened Plastics. London: Applied Science Publ, 1977.
[2] Donald AM, Kramer EJ. J Mat Sci 1982;17:1765.
[3] Haward RN, Owen DRJ. J Mat Sci 1973;8:1136.
[4] Sue H-J, Yee AF. Polymer 1988;29:1619.
[5] Huang Y, Kinloch AJ. J Mat Sci 1992;27:2753.
[6] Steenbrink AC, Van Der Giessen E, Wu PD. J Mech Phys Solids 1997;45:405.
[7] Steenbrink AC, Van Der Giessen E. J Mat Sci 1998;33:3163.
[8] Steenbrink AC, Van Der Giessen E. In: de Borst R, Van der Giessen E, editors. Material Instabilities in Solids, J Wiley, 1998:287.
[9] Steenbrink AC, Van Der Giessen E. J Mech Phys Solids 1999;47:843.
[10] Okamoto Y, Miyagi H, Kakugo M, Takahashi K. Macromolecules 1991;24:5639.
[11] Cheng C, Hiltner A, Baer E, Soskey PR, Mylonakis SG. J Mat Sci 1995;30:587.
[12] Kayano Y, Keskkula H, Paul DR. Polymer 1998;39:821.
[13] Borggreve RJM, Gaymans RJ, Eichenwald HM. Polymer 1989;30:78.
[14] Speroni F, Castoldi E, Fabbri P, Casiraghi T. J Mat Sci 1989;24:2165.
[15] Steenbrink AC, Janik H, Gaymans RJ. J Mat Sci 1997;32:5505.
[16] Dijkstra K, Ter Laak J, Gaymans RJ. Polymer 1994;35:315.
[17] Janik H, Gaymans RJ, Dijkstra K. Polymer 1995;36:4203.
[18] Cheng C, Hiltner A, Baer E, Soskey PR, Mylonakis SG. J Appl Polym Sci 1994;52:177.
[19] Haward RN, Thackray G. Proc R Soc Lond 1968;A302:453.
[20] Boyce MC, Parks DM, Argon AS. Mech Mater 1988;7:15.
[21] Wu PD, Van Der Giessen E. J Mech Phys Solids 1993;41:427.
[22] Argon AS. Phil Mag 1973;28:839.
[23] Arruda EM, Boyce MC. J Mech Phys Solids 1993;41:389.
[24] McMeeking RM, Evans AG. J Am Ceram Soc 1982;65:242.